Investigation of allosteric regulation of porcine fructose-1,6-bisphosphatase

by

Jian Lu

A thesis submitted to the graduate faculty

in partial fulfillment of the requirements for the degree of

MASTER OF SCIENCE

Major: Biochemistry

Program of Study Committee:
Herbert J. Fromm, Co-major Professor
Richard B. Honzatko, Co-major Professor
Drena L. Dobbs

Iowa State University

Ames, Iowa

2007

TABLE OF CONTENTS

LIST OF TABLES

LIST OF FIGURES

LIST OF NOMENCLATURE

FBPase: fructose-1,6-bisphosphatase

$F16P_2$: fructose 1,6-bisphosphate

F6P: fructose 6-phosphate

$F16P_2$: fructose 2,6-bisphosphate

AMP: adenosine 5'-monophosphate

ATP: adenosine 5'-triphosphate

Pi: phosphate

Ala: alanine

Leu: leucine

Ile: Isoleucine

Asp: aspartate

NADP+: nicotinamide adenine dinucleotide phosphate, oxidized form

NADPH: nicotinamide adenine dinucleotide phosphate, reduced form

IPTG: isopropyl-1-thio-b-D-galactopyranoside

SDS-PAGE: sodium dodecyl sulfate polyacrylamide gel electrophoresis

Thr: threonine

Val: valine

PFK-1: fructose-6-phosphate 1-kinase

kDa: kilodalton

ACKNOWLEDGMENTS

I would like to thank Dr. Herbert J. Fromm, my major professor, for his guidance and educational experiences offered during the course of work and lab work. Dr. Fromm has been a superb mentor and an excellent example of an academic scientist. I also like to thank Dr. Richard B. Honzatko, another major professor, who provided detailed guidance on this dissertation.

I am grateful to all the former and current members of the Fromm-Honzatko group and all my friends for their support and help extended during the study in Iowa State University.

Finally, I would like to express my gratitude to my parents and my wife, for their love and unconditional support.

ABSTRACT

Porcine Fructose-1,6-bisphosphatase is a homotetramer with four identical subunits. It plays a central role in gluconeogenesis and is tightly regulated by metabolites fructose 2,6-bisphosphate ($F26P_2$) and AMP. Loop 52-72, loop 182-194 and residues 7-11 of the N-terminal segment play important role in the mechanism of catalysis and allosteric inhibition by AMP by retaining a structural hydrophobic region. Disruption of the hydrophobic region will evidently affect the catalysis and regulation of FBPase. Mutation of Thr^{53} reduced the catalysis activity of FBPase, mutation of Thr^{194} eliminated inhibition of AMP due to its low affinity to the enzyme, while double mutation $Thr^{53/194}$ had accumulative effect. Mutation Ala^{10} exhibited biphasic AMP inhibition, an AMP high affinity site which had comparable IC_{50} with wild-type FBPase and an AMP low affinity site which required 3000-fold AMP to reach 50% relative inhibition.

INTRODUCTION

Fructose-1,6-bisphosphatase (D-fructose-1,6-bisphophate 1-phosphohydrase, EC 3.13.11;FBPase) hydrolyzes fructose 1,6-bisphosphate ($F16P_2$) to fructose 6-phosphate (F6P) and inorganic phosphate (P_i)(Figure 1)(1-5). The kinetic data of the wild-type enzyme is shown in Table 1. FBPase, along with fructose-6-phosphate 1-kinase, define a futile cycle in the gluconeogenic/glycolytic pathways (Figure 2)(6,7). FBPase plays a central role in gluconeogenesis, and is tightly regulated by metabolites fructose 2,6-bisphosphate ($F26P_2$) and AMP, both of which inhibit FBPase, while simultaneously activating fructose-6-phosphate 1-kinase(Figure 3)(5,7). FBPase requires divalent cations (Mg^{2+}, Mn^{2+}, and/or Zn^{2+}) for activity, and certain monovalent cations (K^+, NH_4^+, and Tl^+) further enhance catalysis(3,4). The divalent cation Mg^{2+} sigmoidally increases enzyme activity at pH 7.5 with a Hill coefficient of approximate 2; however, the effect is hyperbolic at pH 9.6(8,9). AMP, binding to an allosteric site, inhibits FBPase with a Hill coefficient of 2 (8,10). $F26P_2$ biosynthesis and degradation is subject to hormonal control principally by glucagon and insulin (7,11), inhibits FBPase by direct ligation at the active site with a Hill coefficient of unity(3-5). Inhibition of FBPase by AMP is nonlinear and noncompetitive with respect to $F16P_2$, but nonlinear and competitive with respect to essential cations (Mg^{2+}, Mn^{2+}, or Zn^{2+}) (12,13). In contrast, inhibition of FBPase by $F26P_2$ is linear and competitive with respect to $F16P_2$ but noncompetitive with respect to Mg^{2+} and synergistic with AMP. $F26P_2$ can lower the apparent inhibition constant for AMP up to 10-fold by enhancing the binding of AMP to FBPase (14). Because the concentration of AMP *in vivo* is relatively constant, the inhibitory effect of AMP will vary with respect to $F26P_2$ levels.

FBPase is a homotetramer with four identical subunits (M_r = 37,000) (Figure 4). Each subunit has binding sites for $F16P_2$, $F26P_2$, and metal ions, which taken together define the active site, and a distinct allosteric AMP binding site (12,15,16). The closest distance between the AMP binding site and the active site is 28 Å in the same subunit. The four subunits of the tetramer occupy the corners of a rectangle, labeled clockwise: C1 through C4, starting with the upper right-hand corner subunit(17). FBPase exists in at least two distinct conformational states, called R (active) and T (inactive). In the R-state, the four subunits lie in the same plane. Binding of AMP to the allosteric site of FBPase causes a transition from the active R-state to inactive T-state by driving a 17^o rotation of the C1-C2 subunit pair with respect to the C3-C4 subunit pair (17,18) (Figure 5). Recent studies revealed two intermediate or hybrid conformations, R-like (I_R-state) (Figure 6) (19) and T-like (I_T-state) (Figure 7) (20). An understanding of the transition between these hybride states may clarify the mechanism of the conformational changes that occur between the canonical R and T-States.

A region of FBPase known as the "dynamic loop 52-72" plays an important role in the allosteric transition of AMP inhibition, having been observed in three conformational states, engaged, disengaged, and disordered (21). The engaged conformation exists in metal-product complexes of wild-type FBPase in the absence of AMP, in which loop 52-72 interacts with the active site (22-24). The disengaged confirmation occurs in AMP complexes with or without products, in which the disengaged loop is far removed from the active site(22,25). The binding of AMP to its allosteric pocket putatively displaces the loop from the active site, and stabilizes the disengaged loop conformation. The disordered conformations of the dynamic loop have appeared in both the R- and T-states, in which the

loop itself interacts weakly with the rest of the enzyme (19,26,27). Mutations of conserved residues in loop 52-72 have significant effects on catalysis and allosteric inhibition of catalysis by AMP (28,29).

Studies on the dynamic loop 52-72 have revealed its potential on the research of the quaternary transition of FBPase. The mechanism of confirmational change between R-state and T-state of FBPase was elusive until recent studies which revealed the first intermediate state of porcine FBPase: a T-like conformation due to the binding of an allosteric effector to the center of the tetramer(Figure 7)(20). The results of that study increase the likelihood of finding intermediate conformational states of FBPase by crystallization and x-ray diffraction analysis. The study of mutant Ala^{54}→Leu revealed an R-like intermediate conformation (I_R) of FBPase in the presence of AMP (Figure 6)(19). In the presence of AMP, the Leu^{54} enzyme grows in two crystal forms: a T-like conformation which has a disordered dynamic loop and an R-like conformation which has an engaged dynamic loop. In this case, the conformation of the key packing interaction of the disengaged loop 52-72 is disrupted by the mutation of Ala^{54}→Leu in the presence of saturating AMP. The Leu^{54} enzyme has wild-type catalytic properties and retains cooperativity in AMP inhibition but exhibits a 50-fold increase in the IC_{50} for AMP (19). In the I_R-state, the dihedral angle of subunit pair C1-C2 relative to C3-C4 is 3^o, which is between that of the canonical R-state (0^o rotation) and T-state (15^o rotation) and differs from the I_T-state (9^o) (Figure 8)(19). The I_R structure presents the immediate consequences of AMP association in the absence of an allosteric transition and reveals the effect of AMP binding in the absence of a complete quaternary transition. These findings suggest the mechanism by which AMP leverages the allosteric transition in FBPase.

It is well established that the T-state and R-state of structures of FBPase differ by a 17° rotation about a molecular symmetry axis (22). In addition, the subunits in the T- and R-states can adopt different tertiary conformations. The loop 52-72 plays significant role in the confirmational changes. In the R-state conformation, loop 52–72 occupies an engaged conformation or a disordered conformation. In 1989, *Ke et al*. reported the disordered conformation of loop 52–72 in FBPase structures crystallized in the absence of metal activators (30). *Choe et al* later observed the engaged conformation in the context of a product-Zn^{2+} complex of the wild-type enzyme (31). In the T-state of wild-type FBPase, loop 52–72 is in the disengaged conformation and is stabilized by the interactions among T-state FBPase subunits. These interactions involve residues 50–60 of subunit C1 with residues 187–194 and 9–11 of subunit C2 (Figure 9) (21). Point mutations in these structural elements profoundly influence AMP inhibition (32,33), AMP cooperativity (33,34), $F26P_2$ inhibition (32,34), and/or metal affinity (32).

A model for allosteric regulation of AMP inhibition was proposed in 2001 (21). At neutral pH, catalysis will occur if loop 52–72 can cycle between its engaged and disordered conformations. A loop that is always engaged is a dead-end complex. A loop that cannot achieve the engaged conformation results in low metal affinity and little or no activity at neutral pH. Assuming loop 52–72 exchanges between its engaged and disordered conformations, the free energy differences between these conformational states must be small, that is, the R-state maintains small free-energy differences between disordered and engaged conformations of loop 52–72. In contrast, the T-state subunit arrangement selectively stabilizes a new conformation for loop 52–72 (disengaged conformation), which depopulates the disordered/ engaged loop conformations. The decline in the catalytic rate of

T-state FBPase is directly related to the differences in free energy between the engaged/disordered loop conformations and the disengaged loop conformation. For the wild-type enzyme, the free energy difference is large; hence, little or no catalysis occurs. I the case of specific mutants of FBPase that selectively destabilize the disengaged loop conformation, the less the free energy difference, the more populated the engaged/disordered loop conformations are. As a consequence, a measurable level of catalysis occurs. Here, the activity may come from FBPase in the T-state subunit arrangement. The free energy relationships of the model are summarized in Figure 10 (21).

Recent studies on the Ile^{10}→Asp FBPase revealed that FBPase activity may come from the I_T-state (unpublished paper), in which loop 52-72 adopts the engaged conformation. If the dynamic loop cannot form the disengaged conformation due to mutation, then the free-energy levels of the I_T- and T-states may be nearly equal, resulting in substantial activity in the presence of saturating AMP. The mechanism of maintaining the conformation of the dynamic loop in the engaged conformation in the T-state or I_T-state is still unknown.

EXPERIMENTAL PROCEDURES

Materials — $F16P_2$, $F26P_2$, $NADP^+$, and AMP were purchased from Sigma. DNA-modifying and restriction enzymes and T4 polynucleotide kinase, and ligase were from Promega. Glucose-6-phophate dehydrogenase and phosphoglucose isomerase came from Roche Applied Sciences. Cibracon Blue sepharose resin, DEAE sepharose resin, and G-50 resin were purchased from Sigma. Other chemicals were of reagent grade or equivalent. *Escherichia coli* strains BMH 71-18 mutS and XL1-Blue came from Clontech and Stratagene, respectively. The FBPase-deficient *E. coli* strain DF657 came from the Genetic Stock Center at Yale University.

Instruments — Sorvall RC-5B refrigerated superspeed centrifuge (Du Pont Instruments), Sorvall Biofuge Pico centrifuge (Knedro Laboratory Products), SLM 8100C fluorimeter (Spectronic Instruments), CARY 100 Bio UV-Visible spectrophotometer (Varian Analytical Instruments), iCycle Thermal cycler (Bio-Rad), Accumet pH meter 915 (Fisher Scientific).

Mutagenesis of Wild-Type FBPase — Mutations were accomplished by specific base changes in double-stranded plasmid using the Transformer™ site-directed mutagenesis kit (Clontech). The mutagenic primers are as follows:

Thr^{39}→Val: 5’ -GCTCAACTCGCTGTGC**GTC**GCGGTCAAAGCC- 3’
5’ -GGCTTTGACCGC**GAC**GCACAGCGAGTTGAGC- 3’
Thr^{39}→Ile: 5’ -GCTCAACTCGCTGTGC**ATC**GCGGTCAAAGCC- 3’
5’ -GGCTTTGACCGC**GAT**GCACAGCGAGTTGAGC- 3’
Ile^{194}→Thr: 5’ -ATCGGAGAGTTC**ACT**TTGGTGGACAGGGAT- 3’
5’ -ATCCCTGTCCACCAA**AGT**GAACTCTCCGAT- 3’

Ile^{53}→Thr: 5’ -AAGGCGGGC**ACC**GCGCACCTCTATGGAATT- 3’
5’ -AATTCCATAGAGGTGCGC**GGT**GCCCGCCTT- 3’
Ile^{53}→Val: 5’ -AAGGCGGGC**GTC**GCGCACCTCTATGGAATT- 3’
5’ -AATTCCATAGAGGTGCGC**GAC**GCCCGCCTT- 3’
Ile^{194}→Val: 5’ -CGGAGAGTTC**GTT**TTGGTGGACAGGG- 3’
5’ -CCCTGTCCACCAA**AAC**GAACTCTCCG- 3’
Thr^{66}→Gly: 5’ -TCCACGAACGTG**GGA**GGTGATCAAGTGAAG- 3’
5’ -CTTCACTTGATCACC**TCC**CACGTTCGTGGA- 3’
Ile^{53}→Ala: 5’ -CAAGGCGGGC**GCC**GCGCACCTCTATGGAATT- 3’
5’ -AATTCCATAGAGGTGCGC**GGC**GCCCGCCTTG- 3’
Ile^{10}→Ala: 5’ -CGACACCAAT**GCC**GTCACCCTAACCCGC- 3’
5’ -GCGGGTTAGGGTGAC**GGC**ATTGGTGTCG- 3’
Ile^{194}→Ala: 5’ -CGGAGAGTTC**GCT**TTGGTGGACAGGG- 3’
5’ -CCCTGTCCACCAA**AGC**GAACTCTCCG- 3’

(codons for point mutations are underlined in bold typeface)

Mutations and the integrity of the construct were confirmed by sequencing the promoter region and the entire open reading frame. The Iowa State University sequencing facility provided DNA sequences, using the fluorescent dye-dideoxy terminator method.

Expression and Purification Wild-type and FBPase Mutants— Effective protein expression and purification procedures for wild-type and FBPase mutants have been developed (19) and are described below. To avoid contamination of recombinant FBPase by endogenous enzyme, an FBPase-deficient strain of *E.coli* (DF657) is always used in the expression of the enzymes. The culture is collected by centrifuging after growing overnight at 37^{o} C following IPTG inducing when cell density (OD_{600}) reaches 1.0~1.2. Large volumes of cells are broken by the method of the French Press, while small amounts were lysed by sonication. Cell-free extracts of FBPase are subjected to heat treatment (usually 65^{o} C for 5 minutes, temperature and/or time length might be changed depending on different mutant proteins), followed by

centrifugation. This has been shown to be an effective procedure for rapidly and easily eliminating most contaminating proteins with little loss of FBPase catalytic activity. The supernatant solution is then loaded onto a Cibracon Blue sepharose column which had previously been equilibrated with 20 mM Tris-HCl (pH 7.5) + 5 mM $MgCl_2$. The column is then washed with 20 mM Tris-HCl pH 7.5 buffer. Then, enzyme is eluted with a solution of 500 mM NaCl in 20 mM Tris-HCl of the same pH. The protein sample is then subjected to desalting and pH adjustment by applying it to a G-50 column that had been washed with 20 mM Tris-HCl pH 8.3 buffer. The protein sample is then loaded onto a DEAE sepharose column equilibrated with the same buffer. Purified enzyme is eluted by NaCl gradient (0–0.6 M) in 20 mM Tris-HCl pH 8.3, and then applied again to a G-50 column pre-equilibrated by 20 mM Tris-HCl pH 7.5 buffer for desalting and pH adjustment. Purity and protein concentrations of FBPase preparations are subject to be confirmed by SDS-polyacrylamide gel electrophoresis (35) and the Bradford assay (36), respectively. The purity of FBPase preparation is usually 95% or greater.

Kinetic Experiments—Assays for the determination of k_{cat} and specific activity ratios at pH 7.5/9.5 employ the coupling enzymes, phosphoglucose isomerase, and glucose-6-phosphate dehydrogenase (3). The reduction of $NADP^+$ to NADPH was monitored by absorbance at 340nm. Other kinetic assays use the same coupling enzymes but monitored the formation of NADPH by its fluorescence emission at 470 nm using an excitation wavelength of 340 nm. Assays are performed at 22 °C in 50 mM Hepes pH 7.5, or in 50 mM CAPS pH 9.5. Assay solutions contain EDTA and KCl at concentrations of 10 μM and 150 mM, respectively. Initial rates is analyzed with programs written either in MINITAB using an α value of 2.0

(13) or by ENZFITTER (37). The kinetic data for AMP inhibition with respect to Mg^{2+} and $F26P_2$ inhibition with respect to $F16P_2$ were fit to several models, and the parameters associated with the best-fitting models of inhibition are reported below.

RESULTS

Expression and Purification Wild-type and FBPase Mutants—Expression and isolation procedures described in 'Experimental Procedures' provided wild-type and most FBPase mutants at 95% or greater purity as judged by SDS-polyacrylamide gel electrophoresis. Usually, FBPase protein (wild-type or mutant) can be specifically eluted by 20mM Tris-HCl pH 7.5 buffer + 5mM AMP after loading to the Cibracon Blue sepharose column. For some mutants (those with very high K_i values for AMP, the AMP elution is not satisfactory), 0.5M NaCl in 20mM Tris-HCl pH 7.5 buffer was used. Subsequent to this step in the purification procedure, a G-50 column for desalting and AMP removal is required. At pH 8.3, the FBPase protein (wild-type or mutant) binds to DEAE sepharose resins weakly. Protein was eluted at the immediately after the NaCl gradient was initiated; however, some mutant proteins did not bind to the resins. In these cases, a flow-through sample after protein loading and/or a 20mM Tris-HCl pH 8.3 (w/o salt) sample was collected. Figure 11 and Figure 12 show the purification procedure of FBPase I53T (which bound to the DEAE sepharose resin) and I194T (which did not bind to the DEAE sepharose resins), respectively. Both SDS-polyacrylamide gels indicated no proteolysis of the purified enzymes.

Kinetic Experiments—Kinetic parameters for wild-type FBPase are depicted in Table 1. Initial rate kinetic studies employed substrate concentrations saturating with respect to $F16P_2$ (20 μM) and Mg^{2+} (10 times K_a-Mg^{2+}) but not so high as to cause inhibition. Mutants involve alterations in the dynamic loop (loop 52-72), loop 185-194, and the N-terminal segment of recombinant porcine FBPase, which together compose structural elements important for

allosteric regulation of FBPase.

I. Mutations at Ile^{53} and Ile^{194}

Kinetic data for mutant FBPases at residue(s) Ile^{53} and/or Ile^{194} are shown in Table 2. Mutations at residue(s) Ile^{53} and/or Ile^{194} have a decreased turnover number relative to wild-type FBPase. Maximal reduction of k_{cat} occurred when $Isoleucine^{53}$ was mutated to Threonine (5-fold lower relative to wild-type FBPase). Though the ratio of specific activities at pH 7.5 and 9.5 for I53T FBPase is low, the low value does not arise from the proteolysis of that mutant (Figure 11). Other mutants have pH ratios comparable to that of wild-type FBPase indicating that they are free of proteolysis. In addition, this finding is consistent with results from SDS-polyacrylamide gel electrophoresis (data not shown).

The determination of K_m for $F16P_2$ (K_m^{F16P2} in Table 2) at pH 7.5 employed a saturating concentration of Mg^{2+} (5.0 mM) and concentrations of $F16P_2$ ranging from 0.5 to 20 μM. Data were fit to the Michaelis-Menten Equation:

$$v/V_m = S/(K_m^{F16P2} + S)$$

where v is the velocity, V_m is the maximum velocity at saturating concentrations of $F16P_2$, S is the concentration of $F16P_2$, and K_m^{F16P2} is the Michaelis constant for $F16P_2$. The affinity of FBPase for $F16P_2$ decreases slightly for mutant I53T, 2-fold lower for I194T, and has an accumulative effect for the double mutant, FBPase I53/194T. Valine and alanine mutants exhibit no obvious change for K_m of $F16P_2$, except of mutant I194A.

The Hill coefficient for Mg^{2+} was determined at a saturating, but noninhibiting concentration of $F16P_2$ (20 μM) and concentrations of free Mg^{2+} ranging from 0.1 to 5.0 mM. Data were fit to Equation 1,

$$v/V_m = 1/ [1 + (A_{0.5}/A)^n] \quad \text{(Eq. 1)}$$

where v is the velocity, V_m is the maximum velocity at saturating concentrations of $F16P_2$ and Mg^{2+}, A is the concentration of Mg^{2+}, n is the Hill coefficient for Mg^{2+}, and $A_{0.5}$ is the concentration of Mg^{2+} that gives v/V_m of 50%. Mutations at positions 53 lost almost half affinity of Mg^{2+}, while mutations at positions 194 had no obvious change. All mutants tested caused no changes in Mg^{2+} cooperativity.

The Hill coefficient for AMP was determined at saturating $F16P_2$ (20 μM), concentrations of free Mg^{2+} at $A_{0.5}$ of each mutant FBPase, and AMP concentrations ranging from 0 to 50 μM for I53T, I53V, I53A, I194V and I194A, 0 to 200 μM for I194T and I53/194T. Data were fit to Equation 2,

$$v/V_0 = 1/[1 + (I/I_{0.5})^n] \quad \text{(Eq. 2)}$$

where v is the velocity, V_0 is the velocity at an AMP concentration of zero, I is the concentration of AMP, n is the Hill coefficient for AMP, and $I_{0.5}$ is the concentration of AMP that gives v/V_0 of 50%. Obviously, threonine mutations lowered the affinity of FBPase for AMP. The concentrations of AMP that are required for 50% inhibition, increased 5-fold for I53T, 40-fold for I194T, and 15-fold for double mutant I53/194T. $I_{0.5}$ showed a slight increase for I194V, I194A and I53A, but a decrease for I53V. All mutants exhibited both Mg^{2+} and AMP cooperativity.

The kinetic mechanism of AMP inhibition with respect to Mg^{2+} was determined from assays that employed saturating (20 μM) $F16P_2$, five different Mg^{2+} concentrations, and five different AMP concentrations. Mg^{2+} concentrations ranged from $A_{0.5}$ of each mutant FBPase to 5.0 mM. AMP concentrations ranged from 0 to 5-fold $I_{0.5}$ of each mutant FBPase. A model for non-linear competitive inhibition (Equation 3) provided the best result (goodness-of-fit of

<5%),

$$V_m/v=1 + K_a/A^2 + (K_a/K_i^{AMP})\ (I/A)^2 \qquad \text{(Eq. 3)}$$

where v is the velocity, V_m is the velocity at an inhibitor concentration of zero saturating concentrations of $F16P_2$ and Mg^{2+}, A is the concentration of Mg^{2+}, I is the concentration of AMP, K_a is the Michaelis constant for Mg^{2+}, and K_i^{AMP} is the dissociation constant for AMP from the enzyme-inhibitor complex. Equation 3 constrains the Hill coefficients for Mg^{2+} and AMP to 2, consistent with independent determinations of these quantities. These results are identical with independent experiment indicating that complete AMP inhibition for threonine mutants requires more AMP than for the wild-type enzyme.

$F26P_2$ is a substrate analog that binds at the active site of the enzyme. The kinetic mechanism of $F26P_2$ inhibition with respect to $F16P_2$ was determined from assays that employed saturating Mg^{2+} (5 mM), five different concentrations of $F16P_2$ (ranging from 1 to 5-time of K_m^{F16P2}), and five different concentrations of $F26P_2$ (0–1 μM for I53V and 0–5 μM for others). A model for linear competitive inhibition provided the best fit to the data (goodness-of-fit of <5%),

$$V_m/v=1 + K_b/B + (K_b/K_i^{F26P2})\ (I/B) \qquad \text{(Eq. 4)}$$

where V_m is the velocity at an inhibitor concentration of zero and saturating concentrations of $F16P_2$ and Mg^{2+}, B is the concentration of $F16P_2$, I is the concentration of $F26P_2$, K_b is the Michaelis constant for $F16P_2$, and K_i^{F26P2} is the dissociation constant for $F26P_2$ from the inhibitor-enzyme complex. The mechanism of $F26P_2$ inhibition is the same for all mutants and wild-type FBPase.

II. Ile^{10}→Ala mutant FBPase

Kinetic parameters for Ile^{10}→Ala mutant FBPase are depicted in Table 3. AMP inhibition for the I10A mutant is biphasic (Figure 13). Complete AMP inhibition of I10A requires ~1000-fold more AMP than for the wild-type enzyme. The biphasic curves of the I10A mutant exhibited that there existed two AMP affinity sites: a high affinity site and a low affinity site. The biphasic curve of the I10A mutant were fit to Equation 5,

$$v=A/[1 + (I/IC_{50\text{-high}})^{n1}] + B/[1 + (I/IC_{50\text{-low}})^{n2}] \qquad \text{(Eq. 5)}$$

where *v* is the velocity, A and B respectively represent the percentage of high and low affinity sites contribution to the inhibition of enzymatic activity, *I* is the concentration of AMP, $IC_{50\text{-high}}$ and $IC_{50\text{-low}}$ respectively represent concentrations of AMP that cause 50% relative inhibition due to the ligation of high and low affinity sites, *n1* and *n2* are Hill coefficients for the high and low affinity sites, respectively. The high affinity site contributed 84% to the inhibition of enzymatic activity and the low affinity contributed 16%. Concentration of AMP that cause 50% relative inhibition due to the ligation of high affinity site ($IC_{50\text{-high}}$) was 0.82±0.02 μM with Hill coefficient 1.45±0.03. $IC_{50\text{-low}}$ was 3070±403μM with Hill coefficient 0.73±0.09. $IC_{50\text{-high}}$ of mutant I10A is comparable with the IC_{50} of wild type FBPase, while $IC_{50\text{-low}}$ is 3000-fold higher than the IC_{50} of wild type FBPase. Elimination of the high affinity AMP site causes the enzyme to lose its cooperative.

The kinetic mechanism of AMP inhibition with respect to Mg^{2+} was determined from assays that employed saturating (20 μM) $F16P_2$ at five different Mg^{2+} concentrations, and five different AMP concentrations. Mg^{2+} concentrations ranged from 1.0 to 5.0 mM. AMP concentrations ranged from 0 to 10 μM. When AMP is absence, the Mg^{2+} is shown as cooperative (Figure 14-A) with a Hill coefficient of 2; whereas by the presence of AMP, the cooperativity of Mg^{2+} is eliminating, and Hill coefficient of Mg^{2+} is 1 when the concentration

AMP presented at 10 μM (Figure 14-B). The loss of Mg^{2+} cooperativity had been observed previously in a 10DEL mutant(21) which appeared a similar biphasic curve with respect of AMP inhibition. The kinetic mechanism of $F26P_2$ inhibition with respect to $F16P_2$ is linear competitive.

In the absence of AMP, the Hill coefficient for Mg^{2+} is approximately 2 (Table 3); however, when AMP is bound to FBPase, Mg^{2+} binding loses its cooperativity (Figure 14). These findings suggest that in the case of the Ile^{10}→Ala mutation communication between subunits (cooperativity) is lost. An additional consequence of AMP binding to the enzyme is the intrasubunit loss of Mg^{2+} cooperativity.

DISCUSSION

Crystal structures of wild-type and various FBPase mutants have shown that loop 52-72 plays a significant role in the function of FBPase. It is for this reason that investigations of this dynamic loop have been a focus of intense research (21-25). Most recently, the discovery of an R-like conformation in the presence of saturating AMP has attracted attention (19). In the presence of saturating AMP, Leu^{54}→Ala mutant FBPase grew in two crystal forms: a T-like conformation with a disordered dynamic loop and an R-like confirmation with an engaged dynamic loop. This intermediate conformation could be the initial step of the quaternary transition of FBPase induced by AMP. In the R-state of FBPase, as shown in Figure 15, residues near the hinge of the engaged dynamic loop in subunit C4, loop 182-194 of subunit C3, and residues 7-11 of the N-terminal segment preceding helix H1 of subunit C3, tightly pack together composing a sandwich model. The hydrophobic side chains at position 53 and 194 are critical to the stability of the engaged conformation of loop 52-72 in the R-state, and thus the catalysis function of FBPase.

The pH-activity ratio of the Thr^{53} mutant is lower than that of the wild-type enzyme. Usually the low pH ratio is considered to be the criterion of FBPase proteolysis *i.e.,* the truncation of 25 residues from the N terminal (38) and/or the proteolysis of loop 52-72 (39). However, the results from SDS-polyacrylamide gel electrophoresis of the pure Thr^{53} enzyme did not exhibit any evidence of enzyme proteolysis. Instead, the 5-fold decrease in k_{cat} indicates that it may be difficult for loop 52-72 to achieve an engaged conformation in the R-state of the Thr^{53} construct. The lower pH-activity ratio effect was also observed with other mutant FBPases (21,32). The effects of the Thr53 mutant can be explained by the importance

of the hydrophobic packing shown on Figure 15. The mutation of Ile^{53} to threonine disrupted the hydrophobic environment in the packing sandwich model which is important to the stability of the engaged confirmation of loop 52-72 in the R-state. Other mutants at position 53, which did not change the hydrophobic packing, are essentially identical to wild-type FBPase.

Unlike the Thr^{53} mutant, the Thr^{194} mutant significantly alters the AMP allosteric regulation of FBPase. Although there was 5-fold increase of K_i^{AMP} for the Thr^{53} mutant, mutant Thr^{194} elevated the K_i^{AMP} approximately 1000-fold relative to wild-type FBPase. As shown on Figure 9, the hydrophobic space which is composed of Ile^{10}, Ile^{59}, and Ile^{194} is important for stabilization of the disengaged confirmation of loop 52-72 in T-state of FBPase. The mutation Ile^{194} to threonine disrupts the hydrophobic environment and in so doing destabilizes the disengaged confirmation of the dynamic loop which ultimately reduces the affinity of the enzyme for AMP. Compared with Ile^{194}, residue Ile^{53} has less effect on allosteric inhibition by AMP. Without causing disruption of the hydrophobic environment, mutant I194V has no obvious effect on the affinity the enzyme for AMP. As expected, the double mutant Ile53/194Thr has complex effects on FBPase properties, *i.e.*, the low pH-activity ratio might originate from the residue 53 and a decrease on the AMP affinity could well stem from residue 194.

Although residues 10 and 194 both play important role in allosteric regulation in the T-state FBPase, they have different effects on the affinity of the enzyme for AMP. While the I194T mutant requires much more AMP to reach 50% inhibition relative to wild-type FBPase, this is not the case with the I10A mutant. Mutant I10A reveals biphasic AMP inhibition (Fig. 13). The $IC_{50\text{-high}}$ of the I10A mutant is comparable to that of wild-type

FBPase, but 1000-fold more AMP is required to completely inhibit the catalytic activity of FBPase relative to that of the wild-type enzyme.

As proposed in an earlier report (21), the change between engaged and disordered conformations of loop 52-72 is a major aspect of FBPase catalysis. If a mutant selectively decreases the stability of the disengaged loop conformation in the T-state, the engaged/disordered conformation ratio may increase and a measurable level of catalysis could be observed in T-state of FBPase. Mutant FBPases with biphasic AMP inhibition have this potential. As noted above, the hydrophobic side chain at these positions is critical to the stability of the disengaged conformation of loop 52-72 in the T-state. Mutant I10D exhibited biphasic AMP inhibition and the crystal structure of its AMP/Zn^{2+} complexes provided an engaged dynamic loop in a T-like quaternary state (unpublished data). That is the first example of an engaged dynamic loop in a T-like quaternary state. The I10A mutant, which exhibited biphasic AMP inhibition identical to that observed with the I10D mutant, could have a conformation similar to that of the I10D mutant, *i.e.*, an engaged dynamic loop in the presence of AMP which could be in a T-like state or in a canonical T-state.

GENERAL CONCLUSIONS

The work described in this thesis contributes to understanding the allosteric regulatory mechanism of Porcine Fructose-1,6-bisphosphatase. The kinetic characterization of mutant FBPases in residues 53 and 194 revealed two important structural information of the regulatory mechanism of FBPase. First, the hydrophobic side chains at position 53 and 194 are critical to the stability of the engaged conformation of loop 52-72 in the R-state, and thus the catalysis function of FBPase. Second, the hydrophobic environment established by residue 10, 59, and 194 in the presence of AMP are critical to the AMP allosteric regulation of FBPase. The dynamic loop of 52-72 plays an important role on the allosteric regulation of FBPase, so lot of works have been done within this region. However, loop 182-194 and residues 7-11 of the N-terminal segment also involve into the allosteric regulation of FBPase by retaining hydrophobic environment both in R-state and T-state of FBPase. Disruptions of the hydrophobic environment have important effects on the catalytic and/or regulatory properties of FBPase. Replacing the hydrophobic residue isoleucine to a hydrophilic residue threonine at position 53 and/or 194 disrupted the hydrophobic sandwich structure of FBPase in the absence of AMP, and thereby reduced the catalytic activity of FBPase. Mutant Ile^{194}→Thr further affected the AMP affinity by disrupting the hydrophobic pocket composed by residues Ile10, Ile59, Ile194 in the presence of AMP. Double mutant $Ile^{53/194}$→Thr had accumulative effect. Further work on crystallography of these mutants will be an important advance and should exhibit us more valuable information and detail. Also we can expect that disrupting the hydrophobic pocket by mutating Ile59 should reveal similar phenomenon.

Residue 10 also plays important role in allosteric regulation in the T-state FBPase, but it has different effect on the AMP affinity with residue 194. Ile^{10}→Ala mutant FBPase revealed biphasic AMP inhibition, which is identical with other mutants done so far in residue 10, indicating that residue 10 plays important role on the communication of AMP binding to FBPase. In high affinity site of Ile^{10}→Ala mutant FBPase, the IC_{50} of AMP to the enzyme is comparable to that of wild-type FBPase; while 3000-fold low in the low affinity site. Meanwhile, mutant I10A lost its AMP cooperativity. Noticeably, Mg^{2+} cooperativity was also eliminated when both AMP and Mg^{2+} were present simultaneously, although Mg^{2+} exhibited cooperative in the absence of AMP. This phenomenon could be a consequence of the intrasubunit loss of Mg^{2+} cooperativity when AMP binding to the enzyme and need additional work to support.

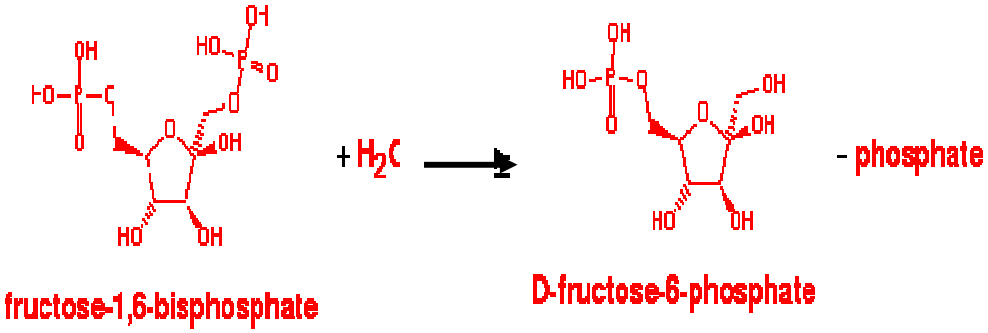

Figure 1. Schematic of the reaction FBPase catalyzes.

Table 1. Kinetic parameters for wild-type FBPase.

	Wild type
Activity ratio, pH 7.5:9.5	3.2 ±0.1
k_{cat} (s^{-1})	20.5±0.6
K_m^{F16P2} (μM)	1.39±0.11
$A_{0.5}$ (mM)	0.90±0.04
Hill coefficient Mg^{2+}	1.82±0.16
$I_{0.5}$ (μM)	1.48±0.02
Hill coefficient AMP	1.90±0.04
K_a (mM^2)	1.31±0.21
K_i^{AMP} (μM^2)	1.66±0.29
K_b (μM)	1.83±0.23
K_i^{F26P2} (μM)	0.22±0.03

The kinetic mechanism of AMP inhibition with respect to Mg^{2+} fits a model for non-linear competitive inhibition:
$V_m/v = 1 + K_a/A^2 + (K_a/K_i^{AMP})\ (I/A)^2$

The kinetic mechanism of $F26P_2$ inhibition with respect to $F16P_2$ fits a model for linear competitive inhibition:
$V_m/v = 1 + K_b/B + (K_b/K_i^{F26P2})\ (I/B)$

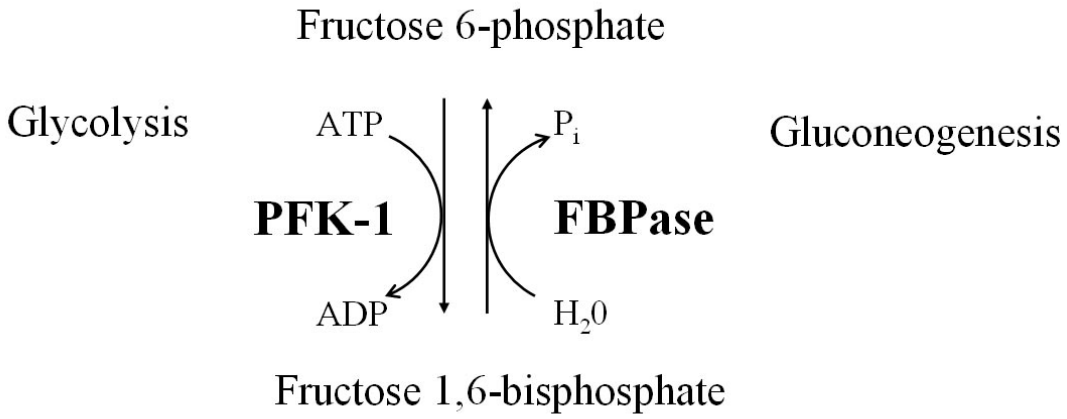

Figure 2. A futile cycle defined by FBPase and fructose-6-phosphate 1-kinase in the gluconeogenic/ glycolytic pathways.

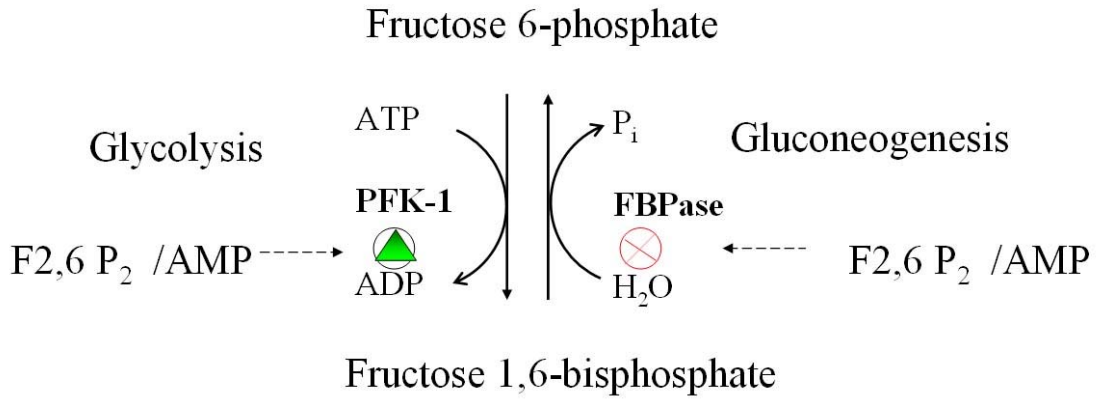

Figure 3. Regulation of FBPase and PFK-1 by $F26P_2$ and AMP.

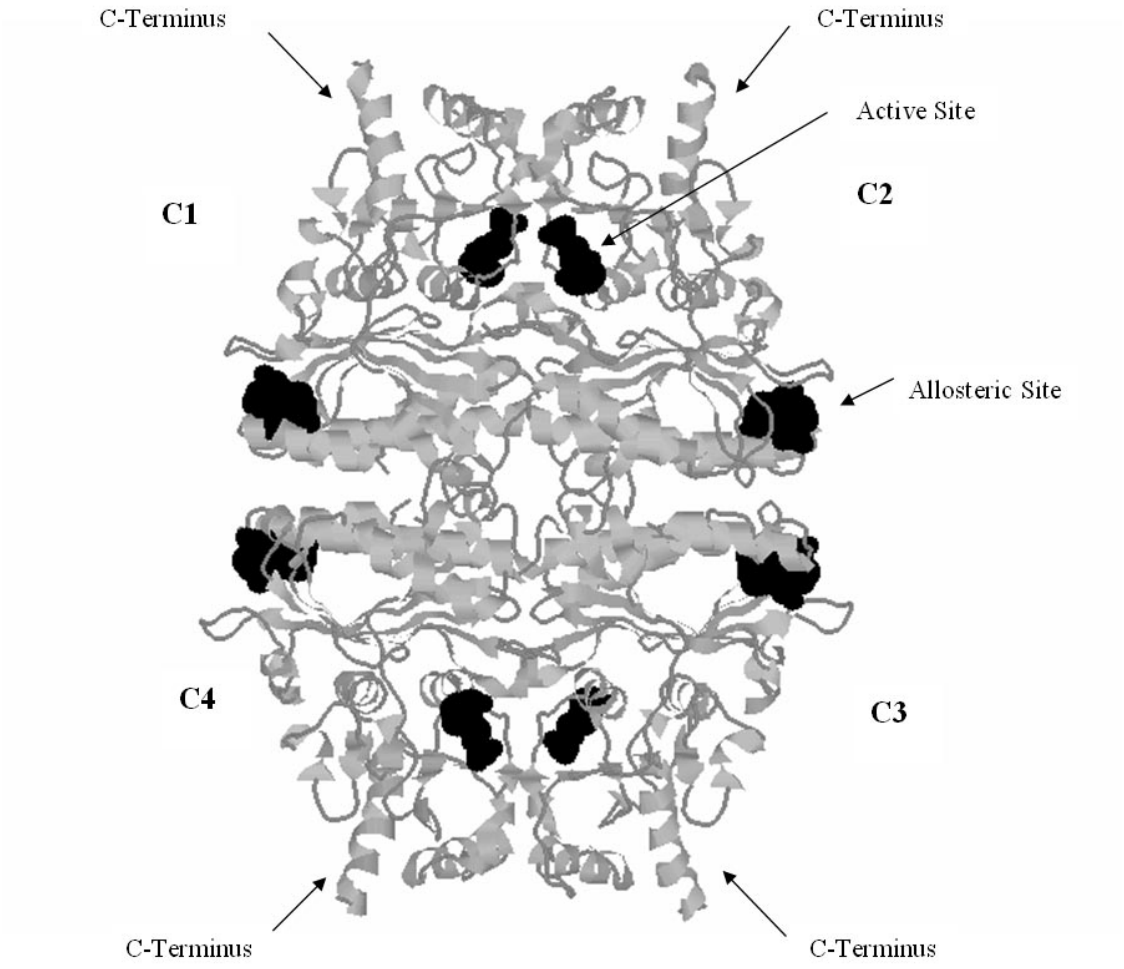

Figure 4. Schematic of the homotetramer conformation of FBPase.

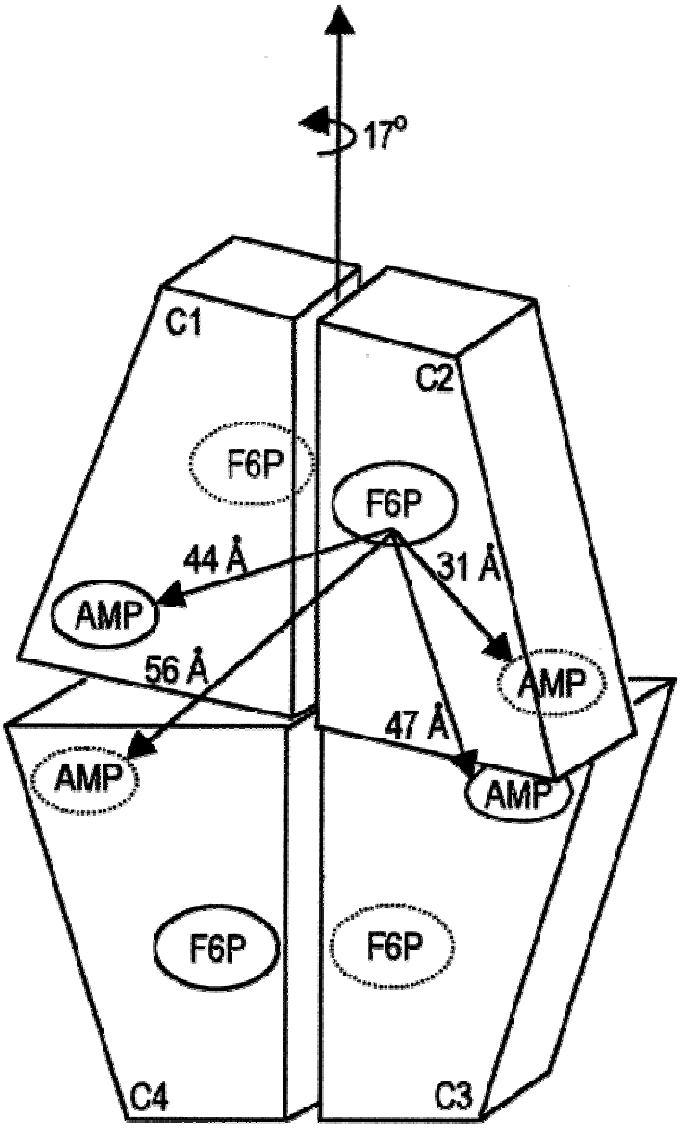

Figure 5. Schematic of the T-state conformation of FBPase. A rotation of the subunit pair C1-C2 by 17° as shown transforms the T-state into the R-state conformer. Dotted ovals represent ligand binding sites on faces of the tetramer hidden from view. Distances measured from atom C-2 of F6P of subunit C2 to atoms C-1' of four bound AMP molecules are presented.

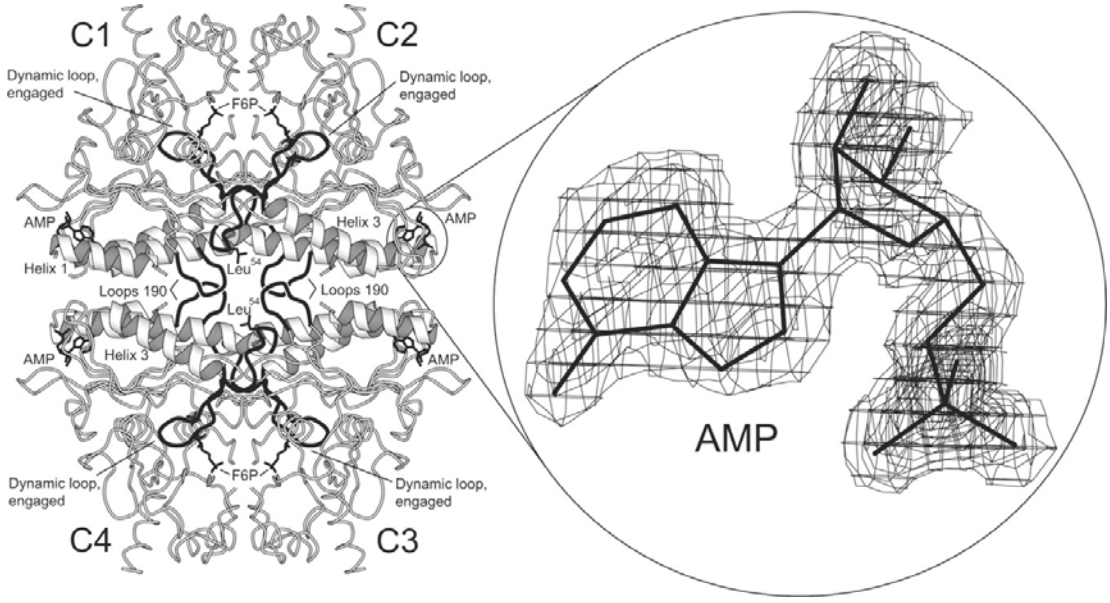

Figure 6. Overview of the R-like (I_R) AMP-product complex of Leu^{54} FBPase.

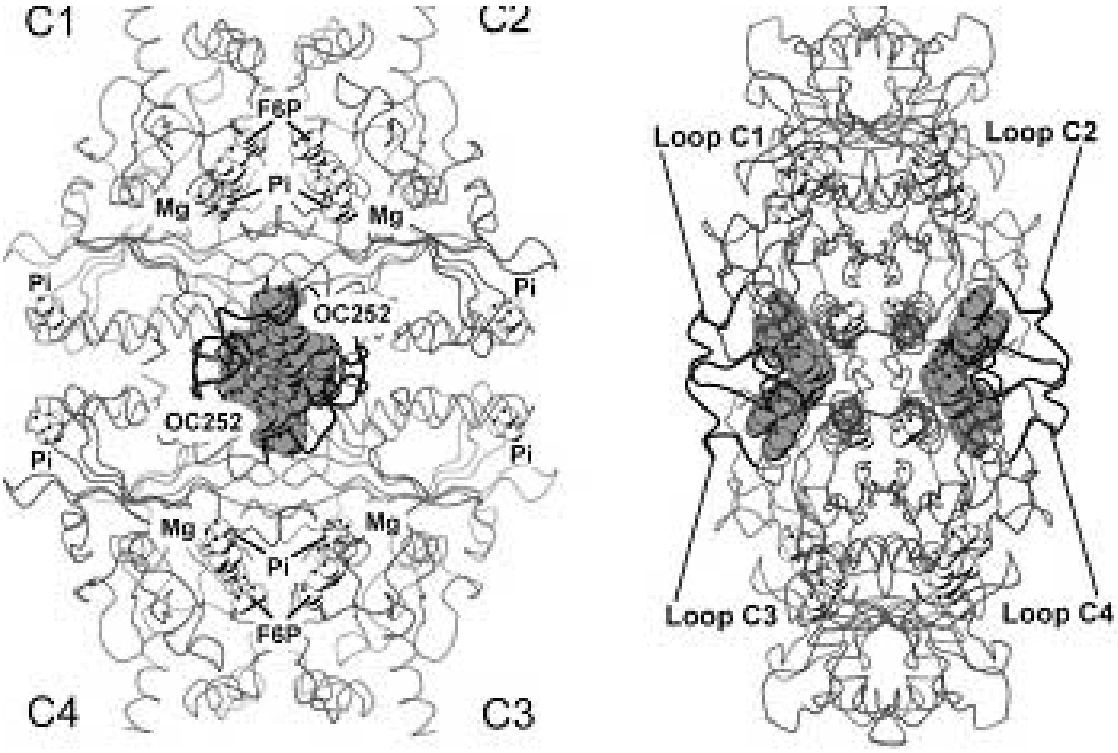

Figure 7. Overview of the T-like (T_R) OC252-FBPase complex.

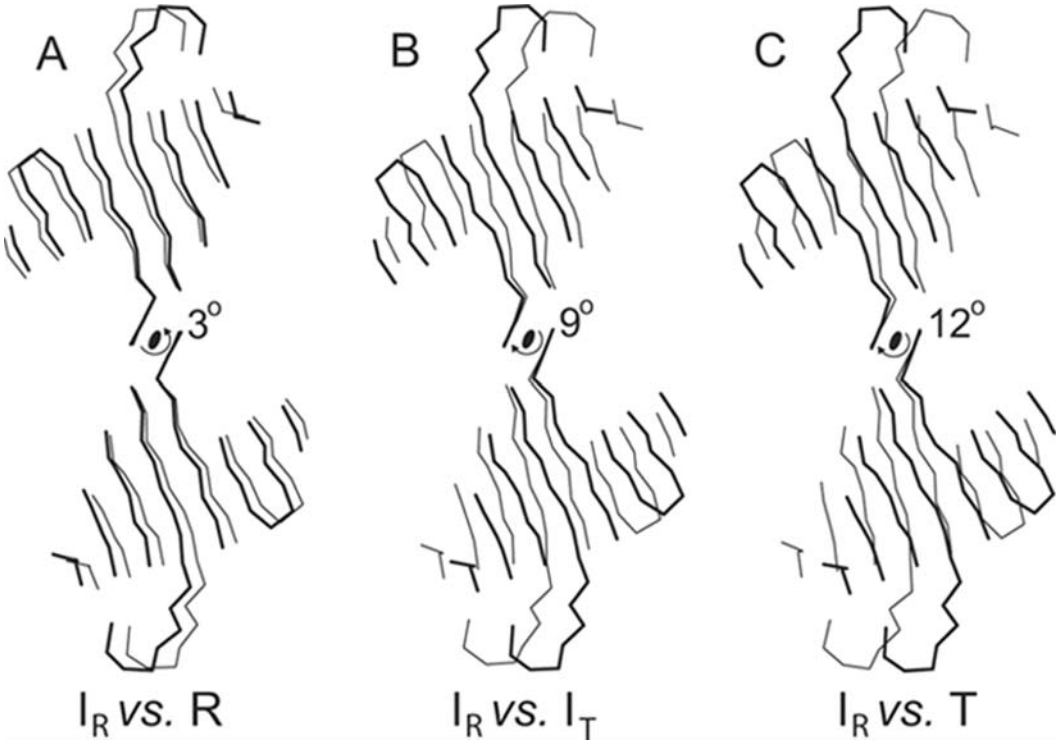

Figure 8. Quaternary states of FBPase.

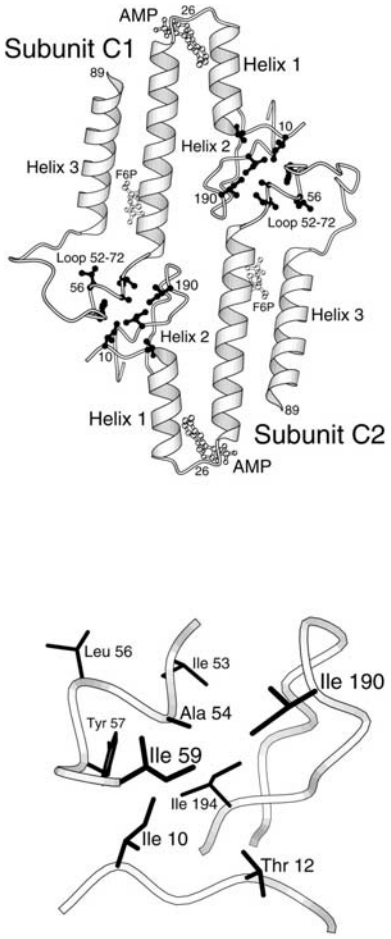

Figure 9. Structural elements important to allosteric regulation in the T-state of FBPase.

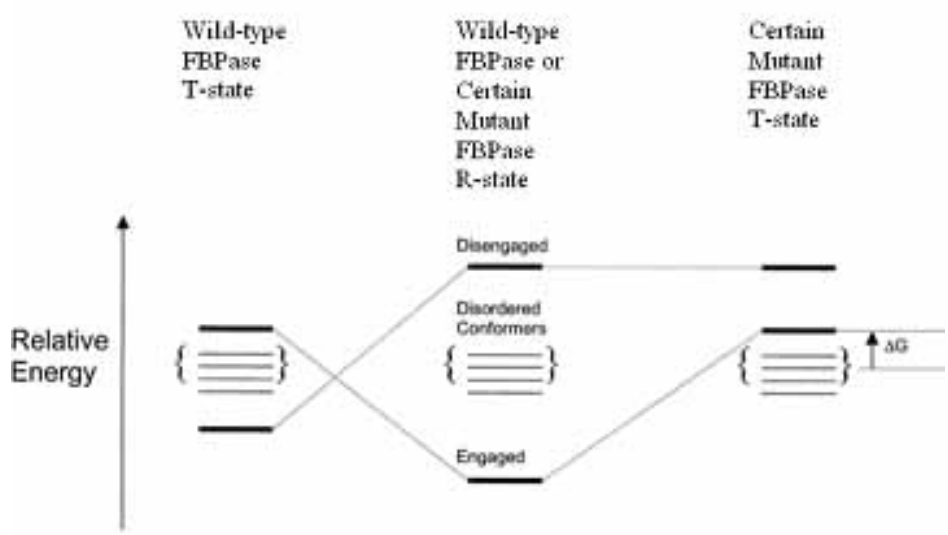

Figure 10. Changes in relative free energy levels of three loop conformations in the R- and T-states of wild-type and mutant FBPases.

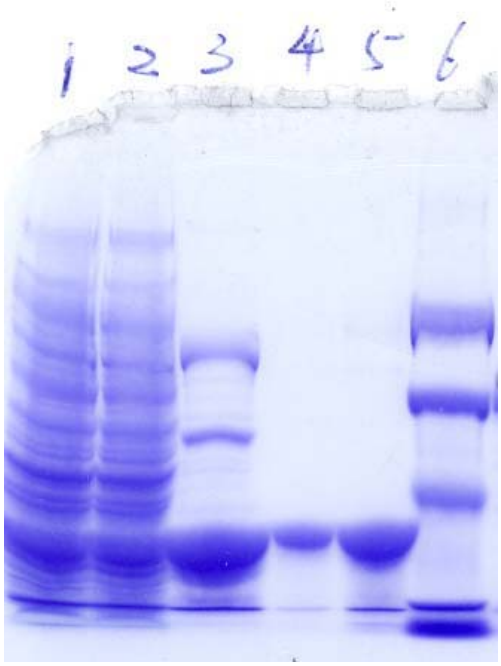

Figure 11. Samples for I53T purification (10% SDS-PAGE). 1. Crude enzyme; 2. After heating treatment; 3. Cibracon Blue; 4. DEAE-sepharose; 5. G-50; 6. Bio-Rad Low Range marker (97kDa,66,45,31,21.5,14.4).

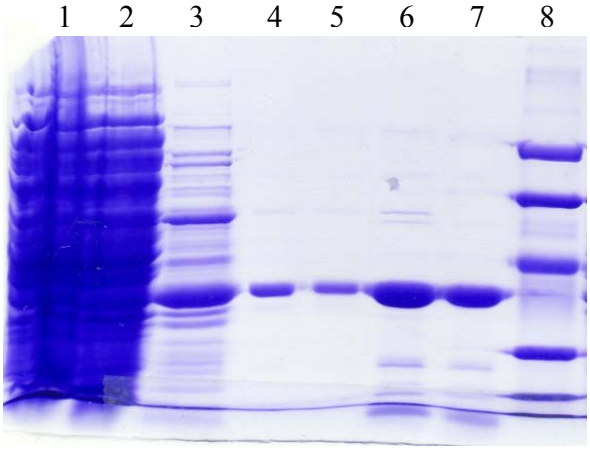

Figure 12. Samples for I194V purification (10% SDS-PAGE). 1. Crude enzyme; 2. After heating treatment; 3. Cibracon Blue; 4. DEAE-sepharose; 5. G-50; 6. DEAE flow through; 7. DEAE wash out; 8. Bio-Rad Low Range marker (97kDa,66,45,31,21.5,14.4).

Table 2. Kinetic parameters for wild-type and mutant FBPase (Ile^{53} and Ile^{194}).

	Wild type	Ile53 - Thr	Ile194 - Thr	Ile53/194 - Thr	Ile53 - Val	Ile194 - Val	Ile53 - Ala	Ile194 - Ala
Activity ratio, pH 7.5:9.5	3.2 ±0.1	1.87±0.04	3.08±0.14	2.02±0.04	3.47±0.14	3.54±0.01	3.50±0.21	2.91 ±0.04
k_{cat} (s^{-1})	20.5±0.6	4.40	10.69	10.94±0.04	15.16±0.04	14.03 ±1.48	9.38±0.18	13.2 ±0.8
K_m^{F16P2} (μM)	1.39±0.11	1.95±0.19	2.60±0.20	3.41±0.35	1.74±0.17	1.93±0.37	1.73±0.20	2.45±0.32
$A_{0.5}$ (mM)	0.90±0.04	1.61±0.08	1.05±0.05	2.30±0.14	1.85±0.14	1.14±0.10	2.30±0.11	1.21±0.07
Hill coefficient Mg^{2+}	1.82±0.16	1.78±0.14	2.04±0.17	2.00±0.21	1.7±0.16	1.49±0.15	1.79±0.12	1.91±0.20
$I_{0.5}$ (μM)	1.48±0.02	6.13±0.21	58±4	22±3	1.00±0.06	4.04±0.07	3.88±0.13	3.63±0.30
Hill coefficient AMP	1.90±0.04	2.16±0.15	1.80±0.16	1.41±0.22	1.58±0.11	2.35±0.10	1.98±0.12	1.62±0.19
K_a (mM^2)	1.31±0.21	2.07±0.44	0.76±0.13	1.11±0.61	2.28±0.64	0.37±0.19	1.58±0.60	0.88±0.20
K_i^{AMP} (μM^2)	1.66±0.29	8.57±2.26	1152±211	96±52	0.22±0.06	1.31±0.72	1.49±0.57	2.38±0.54
K_b (μM)	1.83±0.23	2.56±0.16	1.50±0.14	1.45±0.3	1.4±0.2	1.80±0.24	1.41±0.18	2.14±0.18
K_i^{F26P2} (μM)	0.22±0.03	0.26±0.02	0.47±0.04	1.23±0.09	0.08±0.01	0.22±0.03	0.18±0.02	0.21±0.02

The kinetic mechanism of AMP inhibition with respect to Mg^{2+} fits a model for non-linear competitive inhibition:
$V_m/v = 1 + K_a/A^2 + (K_a/K_i^{AMP})\ (I/A)^2$

The kinetic mechanism of $F26P_2$ inhibition with respect to $F16P_2$ fits a model for linear competitive inhibition:
$V_m/v = 1 + K_b/B + (K_b/K_i^{F26P2})\ (I/B)$

Table 3. Kinetic parameters for wild-type and mutant FBPase (I10A).

	Wild type	Ile10 - Ala
Activity ratio, pH 7.5:9.5	3.2 ±0.1	3.14±0.13
k_{cat} (s^{-1})	20.5±0.6	6.79±0.50
K_m^{F16P2} (μM)	1.39±0.11	1.42±0.18
$A_{0.5}$ (mM)	0.90±0.04	1.43±0.05
Hill coefficient Mg^{2+}	1.82±0.16	1.95±0.10
$I_{0.5}$ (μM)	1.48±0.02	0.82±0.02[a]
Hill coefficient AMP	1.90±0.04	1.45±0.03[a]
K_b (μM)	1.83±0.23	1.67±0.31[b]
K_i^{F26P2} (μM)	0.22±0.03	0.033±0.005[b]

[a] Data reported is for the high affinity site, IC_{50} for low affinity site is 3.07±0.40 mM.
[b] The kinetic mechanism of $F26P_2$ inhibition with respect to $F16P_2$ fits a model for linear competitive inhibition:
$V_m/v = 1 + K_b/B + (K_b/K_i^{F26P2})\ (I/B)$

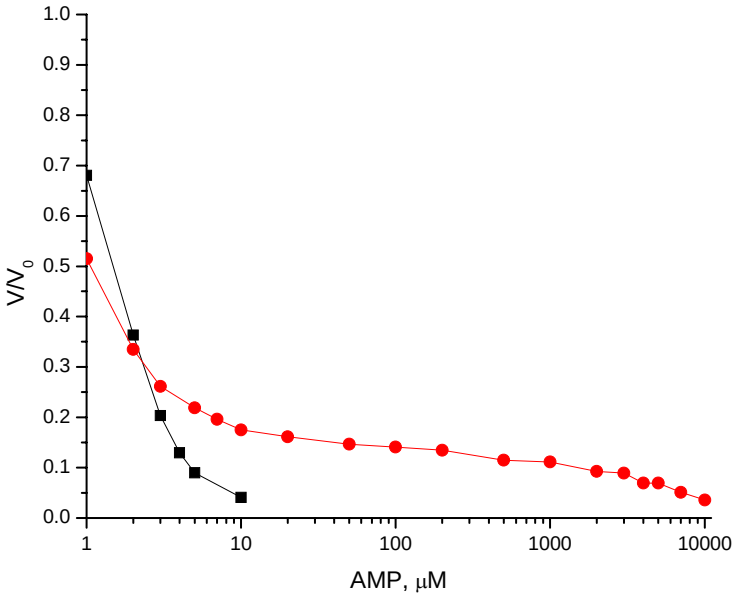

Figure 13. AMP inhibition of wild-type and mutant FBPases. AMP titrations are of wild-type (■), and Ile10Ala (●) FBPases in saturating $F16P_2$ (20 μM) and an Mg^{2+} concentration equal to the Ka for Mg^{2+} of each enzyme.

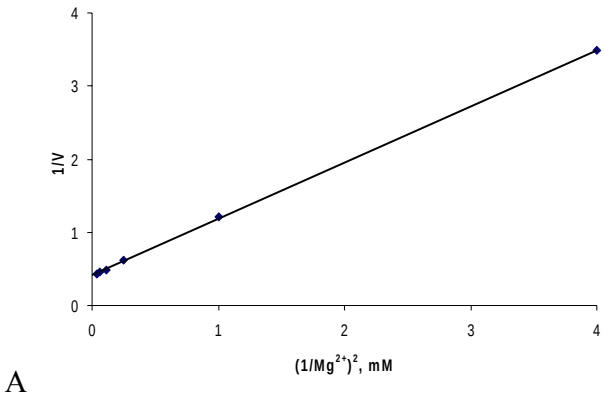

A

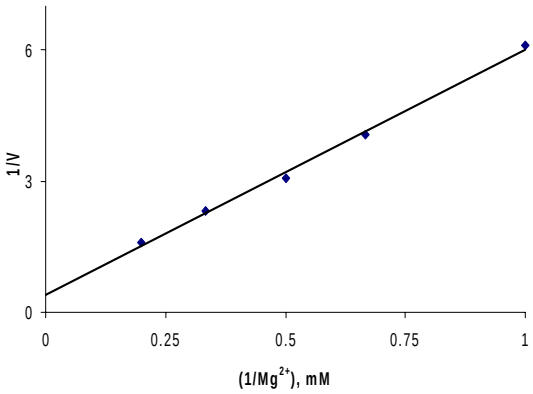

B

Figure 14. Mg^{2+} cooperative behavior of Ile10-Ala mutant FBPase. Hill coefficient of Mg^{2+} is 2 in the absence of AMP (A); Mg^{2+} cooperativity is eliminated (Hill coefficient=1) when concentrations of AMP is 10 μM (B).

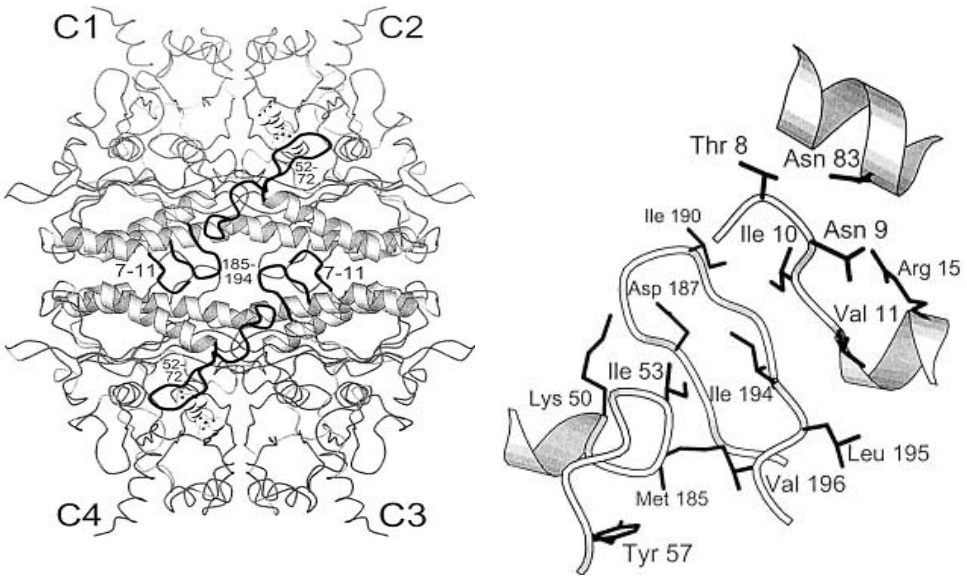

Figure 15. Structural elements important to allosteric regulation in the R-state of FBPase.

REFERENCE

1. Krebs, H. A. (1963) *Advances in Enzyme Regulation (Weber, G., Ed.)* **1**, 385-400, Pergamon Press Ltd., London

2. Marcus, F. (1981) *The Regulation of Carbohydrate Formation and Utilization in Mammals*, (Veneziabe, C. M., Ed.) pp 269-290, University Park Press, Baltimore

3. Benkovic, S. T., & de Maine, M. M. (1982) *Adv. Enzymol. relat. Areas Mol. Biol.* **53**, 45-82

4. Tejwani, G. A. (1983) *Adv Enzymol Relat Areas Mol Biol* **54**, 121-194

5. Van Schaftingen, E. (1987) *Adv Enzymol Relat Areas Mol Biol* **59**, 315-395

6. Kraus-Friedmann, N. (1984) *Physiol Rev* **64**(1), 170-259

7. Pilkis, S. J., el-Maghrabi, M. R., and Claus, T. H. (1988) *Annu Rev Biochem* **57**, 755-783

8. Nimmo, H. G., and Tipton, K. F. (1975) *Eur J Biochem* **58**(2), 567-574

9. Nimmo, H. G., and Tipton, K. F. (1975) *Eur J Biochem* **58**(2), 575-585

10. Stone, S. R., and Fromm, H. J. (1980) *Biochemistry* **19**(4), 620-625

11. Okar, D. A., and Lange, A. J. (1999) *Biofactors* **10**(1), 1-14

12. Ke, H. M., Zhang, Y. P., and Lipscomb, W. N. (1990) *Proc Natl Acad Sci U S A* **87**(14), 5243-5247

13. Liu, F., and Fromm, H. J. (1990) *J Biol Chem* **265**(13), 7401-7406

14. Pilkis, S. J., El-Maghrabi, M. R., Pilkis, J., and Claus, T. (1981) *J Biol Chem* **256**(8), 3619-3622

15. Ke, H. M., Zhang, Y. P., Liang, J. Y., and Lipscomb, W. N. (1991) *Proc Natl Acad Sci U S A* **88**(8), 2989-2993

16. Marcus, F., Edelstein, I., Reardon, I., and Heinrikson, R. L. (1982) *Proc Natl Acad Sci U S A* **79**(23), 7161-7165

17. Zhang, Y., Liang, J. Y., Huang, S., and Lipscomb, W. N. (1994) *J Mol Biol* **244**(5), 609-624

18. Shyur, L. F., Aleshin, A. E., Honzatko, R. B., and Fromm, H. J. (1996) *J Biol Chem* **271**(52), 33301-33307

19. Iancu, C. V., Mukund, S., Fromm, H. J., and Honzatko, R. B. (2005) *J Biol Chem* **280**(20), 19737-19745

20. Choe, J. Y., Nelson, S. W., Arienti, K. L., Axe, F. U., Collins, T. L., Jones, T. K., Kimmich, R. D., Newman, M. J., Norvell, K., Ripka, W. C., Romano, S. J., Short, K. M., Slee, D. H., Fromm, H. J., and Honzatko, R. B. (2003) *J Biol Chem* **278**(51), 51176-51183

21. Nelson, S. W., Kurbanov, F. T., Honzatko, R. B., and Fromm, H. J. (2001) *J Biol Chem* **276**(9), 6119-6124

22. Choe, J. Y., Fromm, H. J., and Honzatko, R. B. (2000) *Biochemistry* **39**(29), 8565-8574

23. Choe, J. Y., Nelson, S. W., Fromm, H. J., and Honzatko, R. B. (2003) *J Biol Chem* **278**(18), 16008-16014

24. Choe, J. Y., Iancu, C. V., Fromm, H. J., and Honzatko, R. B. (2003) *J Biol Chem* **278**(18), 16015-16020

25. Xue, Y., Huang, S., Liang, J. Y., Zhang, Y., and Lipscomb, W. N. (1994) *Proc Natl Acad Sci U S A* **91**(26), 12482-12486

26. Ke, H. M., Thorpe, C. M., Seaton, B., Lipscomb, W. N., and Marcus, F. (1990) *J Mol Biol* **212**(3), 513-539

27. Lu, G., Stec, B., Giroux, E. L., and Kantrowitz, E. R. (1996) *Protein Sci* **5**(11), 2333-2342

28. Kurbanov, F. T., Choe, J. Y., Honzatko, R. B., and Fromm, H. J. (1998) *J Biol Chem* **273**(28), 17511-17516

29. Nelson, S. W., Iancu, C. V., Choe, J. Y., Honzatko, R. B., and Fromm, H. J. (2000) *Biochemistry* **39**(36), 11100-11106

30. Ke, H., Thorpe, C. M., Seaton, B. A., Marcus, F., and Lipscomb, W. N. (1989) *Proc Natl Acad Sci U S A* **86**(5), 1475-1479

31. Choe, J. Y., Poland, B. W., Fromm, H. J., and Honzatko, R. B. (1998) *Biochemistry* **37**(33), 11441-11450

32. Nelson, S. W., Choe, J. Y., Honzatko, R. B., and Fromm, H. J. (2000) *J Biol Chem* **275**(39), 29986-29992
33. Lu, G., Giroux, E. L., and Kantrowitz, E. R. (1997) *J Biol Chem* **272**(8), 5076-5081

34. Carcamo, J. G., Yanez, A. J., Ludwig, H. C., Leon, O., Pinto, R. O., Reyes, A. M., and Slebe, J. C. (2000) *Eur J Biochem* **267**(8), 2242-2251

35. Laemmli, U. K. (1970) *Nature* **227**, 680-685

36. Bradford, M. W. (1976) *Anal. Biochem.* **72**, 248-252

37. Leatherbarrow, R. J. (1987) *ENZFITTER: A Non-Linear Regression Data Analysis Program for the IBM PC*, 13-75, Elsevier Science Publishers B. V., Amsterdam

38. Chatterjee, T., Reardon, I., Heinrikson, R. L., and Marcus, F. (1985) *J Biol Chem* **260**(25), 13553-13559

39. Horecker, B. L., Melloni, E., and Pontremoli, S. (1975) *Adv Enzymol Relat Areas Mol Biol* **42**, 193-226